
Differentiable Bayesian Neural Network Inference for Data Streams

Namuk Park, Taekyu Lee, Songkuk Kim
Yonsei University

{namuk.park, taekyu.lee, songkuk}@yonsei.ac.kr

Abstract

While deep neural networks (NNs) do not provide the confidence of its prediction, Bayesian neural network (BNN) can estimate the uncertainty of the prediction. However, BNNs have not been widely used in practice due to the computational cost of inference. This prohibitive computational cost is a hindrance especially when processing stream data with low-latency. To address this problem, we propose a novel model which approximate BNNs for data streams. Instead of generating separate prediction for each data sample independently, this model estimates the increments of prediction for a new data sample from the previous predictions. The computational cost of this model is almost the same as that of non-Bayesian NNs. Experiments with semantic segmentation on real-world data show that this model performs significantly faster than BNNs, estimating uncertainty comparable to the results of BNNs.

1 Introduction

While deterministic neural networks (DNNs) surpass human capability in some area in terms of prediction accuracy [1, 2, 3], it has been unable to estimate the uncertainty of the predictions until recently. Since the prediction can not be perfect and the misprediction might result in fatal consequences in areas such as medical analysis and autonomous vehicles control, estimating uncertainty as well as predictions will be crucial for the safer application of machine learning based systems.

Bayesian neural network (BNN), a neural network (NN) that uses probability distributions as weights, estimates not only predictive results but also uncertainties. This allows computer systems to make better decisions by combining uncertainty with prediction. Moreover, BNN can achieve high performance in a variety of fields, e.g. image recognition [4, 5], reinforcement learning [6, 7], language modeling [8], meta-learning [9, 10], and multi-task learning [11], by exploiting uncertainty.

Although BNNs have these theoretical advantages, they have not been used as a practical tool. The inference speed has detained BNNs from wide applications. BNN executes NN inference for dozens of samples from weight distributions. Since sampling and multiple NN executions are difficult to be parallelized, the inference execution takes an order of magnitude more time. Particularly, this is a significant barrier for processing data streams with low-latency.

Most time-varying data streams change continuously, and so do the predictions of BNNs. We speed up estimating of uncertainty by calculating the increments between two consecutive results, instead of calculating the separate prediction for each input data. To this work, we propose a *differentiable BNN* (DBNN) inference with respect to an input data, and we show that the time complexity of this model is nearly the same as that of DNNs. We evaluated DBNN with semantic segmentation using road scene video sequences and the results show that DBNN has almost no degradation in computational performance compared to DNNs. The uncertainty predicted by DBNN is comparable to that of BNN.

The main contributions of this work are;

- We propose differentiable Bayesian neural network inference with respect to input data as an approximation of the Bayesian neural network inference for data streams. This model is flexible parametric and converts DNN to BNN without significant modifications.
- We theoretically and empirically show that the computational performance of DBNN is almost the same as that of DNN.

2 Related Work

BNNs are a state-of-the-art method to estimate predictive uncertainty while DNNs based approaches have been developed recently [12, 13]. BNNs with probability distributions as weights produce probabilistic results. To make prediction, BNNs sample from the weight probabilities and performs DNN for each sample. In this section, we describe the details and challenges of BNNs inference process.

2.1 Bayesian Neural Network Inference

Suppose that $p(\mathbf{x}^1)$ is posterior probability of NN weights \mathbf{x}^1 and $p(\mathbf{y}|\mathbf{x}^0, \mathbf{x}^1)$ is the BNN model for input data \mathbf{x}^0 . Then, the inference result of BNN is a predictive distribution:

$$p(\mathbf{y}|\mathbf{x}_*^0) = \int p(\mathbf{y}|\mathbf{x}_*^0, \mathbf{x}^1)p(\mathbf{x}^1)d\mathbf{x}^1 \quad (1)$$

where \mathbf{x}_*^0 is observed input data vector and \mathbf{y} is output vector. For simplicity, BNNs are usually modeled to have a probability distribution with the mean of the prediction of DNN [14, 15]:

$$p(\mathbf{y}|\mathbf{x}_*^0, \mathbf{x}^1) = \mathcal{N}(\mathbf{y}|\text{NN}(\mathbf{x}_*^0, \mathbf{x}^1), \tau^{-1}) \quad (2)$$

where $\text{NN}(\cdot)$ is prediction of DNN and τ is a given parameter. (1) can be approximated using Markov chain Monte Carlo (MCMC) [16]:

$$\frac{1}{N_{\mathbf{x}_*^1}} \sum_{\mathbf{x}_*^1} p(\mathbf{y}|\mathbf{x}_*^0, \mathbf{x}_*^1) \quad (3)$$

where $\mathbf{x}_*^1 \sim p(\mathbf{x}^1)$ and $N_{\mathbf{x}_*^1}$ is number of samples. The expectation value of the obtained predictive distribution is the predictive result of BNN and the variance is the predictive uncertainty. However, this approach has the following problems: First, it iteratively computes the DNN. The repetitive computation of NNs is difficult to be parallelized due to various problems, such as memory limitations of the GPU [5], and this results in the decrease of computation speed. Second, MCMCs are slow. Moreover, despite recent achievements [17], it is challenging to achieve linearly scaling performance for multi-GPU MCMC. Third, it is difficult to check for convergence of MCMCs.

2.2 Bayesian Neural Network Gradient

We obtain differentiation of BNN inference (1) with respect to \mathbf{x}_*^0 in this paper. Although it has not been considered before, the differentiation of probabilistic function with respect to \mathbf{x}^1 has been widely investigated to optimize the loss function in the training process of BNN.

It is standard to use a gradient descent approach to optimize the loss function, e.g. evidence lower bound (ELBO) $\mathbb{E}_{p(\mathbf{x}^1)}[\log p(\mathbf{x}^0, \mathbf{x}^1) - \log p(\mathbf{x}^1)]$. Several methods are used to obtain the gradient descent: dropout [15, 18], batch normalization [19], expectation propagation [14], smooth transformation for samples [20, 21, 22, 23, 24, 25], and reparametrization trick [26, 27, 8]. Among them, reparametrization is the most comparable to the method introduced in this paper.

Most loss functions, including ELBO, are expectation over $p(\mathbf{x}^1)$, i.e., $\mathcal{L} = \mathbb{E}_{p(\mathbf{x}^1)}[f(\mathbf{x}^1)]$ for arbitrary functions $f(\cdot)$. As the inference mentioned in (3), the loss function can be approximated using MCMC. However, the approximated \mathcal{L} is not differentiable with respect to \mathbf{x}^1 because the samples depend on \mathbf{x}^1 . To address this issue, reparametrization methods sample a variable ϵ from fixed probability distribution $p(\epsilon)$ and $\mathbf{x}^1 = t(\epsilon)$ where t is a deterministic function. Then, the loss function is expectation over the invariant distribution, i.e., $\mathcal{L} = \mathbb{E}_{p(\epsilon)}[f(\mathbf{x}^1)]$, and the approximated \mathcal{L} becomes differentiable, i.e., $\partial_{\mathbf{x}^1} \mathcal{L} = \mathbb{E}_{p(\epsilon)}[\partial_{\mathbf{x}^1} f(\mathbf{x}^1)]$.

In this paper, we obtain the differentiation of approximated expectation using sampling in a different way. We calculate the expectation for *all* possible samples. Then, we change the importance weights of the samples without changing the positions of samples, so we decide which sample to focus our *attention* on.

3 Online Codevector Histogram

Vector quantization was introduced in [28, 29] in order to compress a probability distribution to a dozens of samples called codevectors. [30] has shown that the histogram of codevectors (combining codevectors with counts) can effectively represent the features of face image dataset. We introduce *online codevector histogram* (OCH) to estimate the probability distribution of data stream as well as dataset. OCH can add a new codevector and delete old ones, while counting the matches of each codevector for the past data stream. OCH maps the input vector to the codevector using nearest neighbor search. Therefore, it is a high-dimensional histogram where the Voronoi diagram is the boundary and a codevector represents the corresponding bin. DBNN uses OCH to approximate the probability distributions of input and output vector data streams.

Algorithm 1 shows OCH algorithm. There are three steps as follows: (a) First, given a new input vector, OCH finds the nearest codevector and increases its count. Then, it divides the corresponding bin by inserting the input vector as a new codevector with probability proportional to the count. (b) Second, OCH decrease all counts by the same rate to reduce the contribution of old data. (c) Third, OCH deletes codevectors with probability in inverse proportion to its counts.

Algorithm 1: Update OCH

input : input vector \mathbf{x}_* , count of input vector n_* , OCH = $\{(\mathbf{c}_i, n_i)\}$, hyperparameters K , λ , and ϕ
output : updated OCH

- 1 $\mathbf{c}_i \leftarrow$ Search the nearest codevector to \mathbf{x}_* in OCH
- 2 $n_i \leftarrow n_i + n_*$ where n_i is count of \mathbf{c}_i
- 3 $p \sim \text{Bernoulli}(\sigma(\pi_i - \bar{\pi} + \phi))$ where $\sigma(\cdot)$ is sigmoid, $N = \sum_i n_i$, $\pi_i = n_i/N$, and $\bar{\pi} = 1/K$
- 4 **if** $p = 1$ **then**
- 5 OCH \leftarrow OCH $\cup \{(\mathbf{x}_*, n_i \times e^{-\lambda/N})\}$
- 6 $n_i \leftarrow n_i \times (1 - e^{-\lambda/N})$
- 7 **forall** $(\mathbf{c}_j, n_j) \in$ OCH **do**
- 8 $n_j \leftarrow n_j \times e^{-\lambda/N}$
- 9 **forall** $(\mathbf{c}_k, n_k) \in$ OCH **do**
- 10 $q \sim \text{Bernoulli}(\sigma(\bar{\pi} - \pi_k + \phi) \cdot \bar{\pi})$
- 11 **if** $q = 1$ **then**
- 12 OCH \leftarrow OCH $\setminus \{(\mathbf{c}_k, n_k)\}$

OCH takes three hyperparameters: K , λ , and ϕ . The algorithm maintains K codevectors on average. λ determines how fast OCH forgets old counts with the rate of $e^{-\lambda/N}$. ϕ with count of each bin regulates the probability of adding and deleting codevectors.

OCH approximates probability distribution $p(\mathbf{x})$ as:

$$p(\mathbf{x}) \simeq \sum_i \pi_i \mathcal{V}(\mathbf{x}|\mathbf{c}_i) \quad (4)$$

where $N = \sum_i n_i$, $\pi_i = n_i/N$, and $\mathcal{V}(\mathbf{x}|\mathbf{c})$ is the bin or *neighborhood* of \mathbf{c} with $\int \mathcal{V}(\mathbf{x}|\mathbf{c})d\mathbf{x} = 1$. The right-hand-side of (4) is clearly differentiable with respect to π while a set of random samples from $p(\mathbf{x})$ is not differentiable. Given a new input data, OCH changes only one count of the nearest codevector. Therefore, if $n_* \ll N$, the difference of OCH for a new input vector is approximately:

$$\delta p(\mathbf{x}) \simeq \sum_i \delta \pi_i \mathcal{V}(\mathbf{x}|\mathbf{c}_i) \quad (5)$$

$$\simeq \alpha \mathcal{V}(\mathbf{x}|\mathbf{c}_*) \quad (6)$$

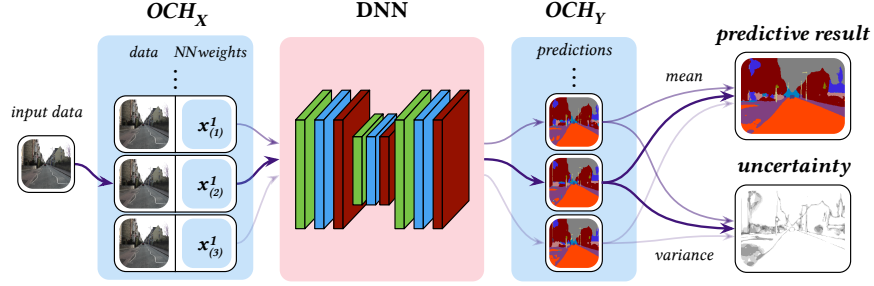


Figure 1: DBNN Inference. OCHs are added to the DNN to estimate the probabilities of input and output vector streams. Given a new data, OCH_X adjusts the weight (arrows) of the nearest codevector of OCH_X representing the input vector stream. DBNN adjusts weights of the codevectors of the OCH_Y representing the predictive distribution based on the results of the inner DNN. DBNN derives predictive result and uncertainty from the weighted ensemble of the codevectors of OCH_Y .

where \mathbf{c}_* is the nearest codevector to the input vector, $\alpha = \delta n / N$, and δn is the difference of the count of \mathbf{c}_* .

Nearest neighbor search is the most computationally intensive when updating OCH for a high-dimensional input vector. To mitigate the computational complexity, we use locality-sensitive hashing with stable distribution, $h = \lfloor (\mathbf{a} \cdot \mathbf{x}_* + b) / w \rfloor$ for a vector \mathbf{a} and scalars b and w . It requires up to $\log K$ hashes for precise search. The upper bound of the computational complexity is $\mathcal{O}(\dim(\mathbf{x}) \log K)$.

4 Differentiable Bayesian Neural Network Inference

When a data stream $\mathcal{D} = \{\dots, \mathbf{x}_*^0\}$ is given, where each subsequent data sample changes continuously, the prediction of a NN for \mathcal{D} also changes continuously, i.e., $p(\mathbf{y}) \rightarrow p(\mathbf{y}) + \delta p(\mathbf{y})$, because a NN (with continuous activation) is a homeomorphism. We show that $\delta p(\mathbf{y})$ is approximately proportional to the prediction of a NN augmented with OCH to the input and output for the recent data \mathbf{x}_*^0 . Figure 1 shows the structure of DBNN, where DNN is augmented with OCHs as distribution estimators of input and output stream. DBNN calculates predictive uncertainty as well as the predictive result using the weighted ensemble of output codevectors.

4.1 Differentiation of Bayesian Neural Network Inference as Difference of Prediction

It is challenging to calculate the difference of (1) for a new data \mathbf{x}_*^0 from \mathcal{D} because the differentiation of right-hand-side of (1) with respect to \mathbf{x}_*^0 is analytically intractable. To address this issue, DBNN introduces a probability of \mathbf{x}^0 given \mathcal{D} into the inference as:

$$p(\mathbf{y}|\mathcal{D}) = \int p(\mathbf{y}|\mathbf{x}^0, \mathbf{x}^1) p(\mathbf{x}^0|\mathcal{D}) p(\mathbf{x}^1) d\mathbf{x}^0 d\mathbf{x}^1 \quad (7)$$

$$= \int p(\mathbf{y}|\mathbf{x}) p(\mathbf{x}|\mathcal{D}) d\mathbf{x} \quad (8)$$

where $\mathbf{x} = (\mathbf{x}^0, \mathbf{x}^1)$ and $p(\mathbf{x}|\mathcal{D}) = p(\mathbf{x}^0|\mathcal{D}) p(\mathbf{x}^1)$. $p(\mathbf{x}^0|\mathcal{D})$ is separately learned with respect to the data stream \mathcal{D} by another model and is called *data uncertainty*. $p(\mathbf{x}^1)$ is the posterior distribution obtained from BNN training and is called *model uncertainty*. DBNN inference decouples data (stream) from the model. On the other hand, it joins the probability of data and the probability of the NN weights, then \mathbf{x}^0 and \mathbf{x}^1 are symmetric. When the most recent data sample is considered instead of the data stream, i.e., $p(\mathbf{x}^0|\mathcal{D}) = \delta(\mathbf{x}^0 - \mathbf{x}_*^0)$ where $\delta(\cdot)$ is the delta function, DBNN inference is reduced to BNN inference.

To calculate (8), we use OCH to represent $p(\mathbf{x}|\mathcal{D})$, i.e., (4), and call it OCH_X , instead of generating samples from $p(\mathbf{x}|\mathcal{D})$ using MCMC:

$$p(\mathbf{y}|\mathcal{D}) \simeq \sum_i \pi_i \int p(\mathbf{y}|\mathbf{x}) \mathcal{V}(\mathbf{x}|\mathbf{c}_i) d\mathbf{x} \quad (9)$$

where π_i is weight of codevector \mathbf{c}_i and proportional to the count of the codevector. $\mathcal{V}(\mathbf{x}|\mathbf{c}_i)$ is neighborhood of \mathbf{c}_i . In order to approximate (8), we adjust the *attentional* focus on samples by changing the weights of the samples instead of changing the samples themselves. Then, $\delta p(\mathbf{y}|\mathcal{D})$ can be approximated by changing the weight of the codevector nearest to \mathbf{x}_*^0 as:

$$\delta p(\mathbf{y}|\mathcal{D}) \simeq \sum_i \delta \pi_i \int p(\mathbf{y}|\mathbf{x}) \mathcal{V}(\mathbf{x}|\mathbf{c}_i) d\mathbf{x} \quad (10)$$

$$\simeq \alpha \int p(\mathbf{y}|\mathbf{x}) \mathcal{V}(\mathbf{x}|\mathbf{c}_*) d\mathbf{x} \quad (11)$$

because $\int p(\mathbf{y}|\mathbf{x}) \mathcal{V}(\mathbf{x}|\mathbf{c}_i) d\mathbf{x}$ is invariant with respect to \mathcal{D} , i.e., $\delta [\int p(\mathbf{y}|\mathbf{x}) \mathcal{V}(\mathbf{x}|\mathbf{c}_i) d\mathbf{x}] = 0$, and (6) holds. We approximate $\mathcal{V}(\mathbf{x}|\mathbf{c}_*)$ distributed near \mathbf{c}_* to distributed only \mathbf{c}_* , i.e., $\mathcal{V}(\mathbf{x}|\mathbf{c}_*) \simeq \delta(\mathbf{x} - \mathbf{c}_*)$:

$$\delta p(\mathbf{y}|\mathcal{D}) \simeq \alpha p(\mathbf{y}|\mathbf{c}_*) \quad (12)$$

It is safe to assume that $p(\mathbf{y}|\mathbf{c}_*)$ is dominantly distributed near $\text{NN}(\mathbf{c}_*)$ because the expected value of \mathbf{y} should be equal to $\text{NN}(\mathbf{c}_*)$:

$$\delta p(\mathbf{y}|\mathcal{D}) \simeq \alpha \mathcal{V}(\mathbf{y}|\text{NN}(\mathbf{c}_*)) \quad (13)$$

where $\text{NN}(\mathbf{c}_*)$ is prediction of DNN for \mathbf{c}_* . In conclusion, the difference of the DBNN prediction contributes only to the neighborhood of the DNN prediction for the codevector in $\text{OCH}_{\mathbf{X}}$ approximately. Thus, given the $\text{OCH}_{\mathbf{Y}}$ representing $p(\mathbf{y}|\mathcal{D})$, $p(\mathbf{y}|\mathcal{D}) + \delta p(\mathbf{y}|\mathcal{D})$ can be approximated by updating the $\text{OCH}_{\mathbf{Y}}$ for the prediction of DNN.

4.2 Implementation of Differentiable Bayesian Neural Network Inference

Algorithm 2 describes the inference process of DBNN, which is composed of three steps as follows: (a) First, the algorithm updates $\text{OCH}_{\mathbf{X}}$ for $\mathbf{x}_* = (\mathbf{x}_*^0, \mathbf{x}_*^1)$ where \mathbf{x}_*^1 is a random sample from given approximated posterior distribution $\text{OCH}_{\mathbf{X}^1}$ which represents $p(\mathbf{x}^1)$. (b) Second, if $\text{OCH}_{\mathbf{X}}$ generated a new codevector in $\text{OCH}_{\mathbf{X}}$, DBNN generates the prediction for the new codevector using DNN and keeps the prediction in a cache table. As a result, the cache table contains the results of DNN corresponding to all codevectors in $\text{OCH}_{\mathbf{X}}$. (c) Third, DBNN finds the nearest neighbor codevector to \mathbf{x}_*^0 in $\text{OCH}_{\mathbf{X}}$, looks up the corresponding prediction in the cache table and update $\text{OCH}_{\mathbf{Y}}$ for the prediction for the codevector.

Algorithm 2: DBNN Inference

input : input data vector \mathbf{x}_*^0 , deterministic neural network $\text{NN}(\cdot)$, posterior distribution $\text{OCH}_{\mathbf{X}^1}$, distribution of input vector $\text{OCH}_{\mathbf{X}}$, distribution of output vector $\text{OCH}_{\mathbf{Y}}$

output : updated distribution of input vector $\text{OCH}_{\mathbf{X}}$, updated distribution of output vector $\text{OCH}_{\mathbf{Y}}$

- 1 $\mathbf{x}_*^1 \sim \text{OCH}_{\mathbf{X}^1}$
 - 2 $\mathbf{x}_* \leftarrow (\mathbf{x}_*^0, \mathbf{x}_*^1)$
 - 3 $\text{OCH}_{\mathbf{X}} \leftarrow \text{Update } \text{OCH}_{\mathbf{X}} \text{ for } \mathbf{x}_*$
 - 4 **if** new codevector \mathbf{c}_i exists in $\text{OCH}_{\mathbf{X}}$ **then**
 - 5 $\mathbf{y}_i = \text{NN}(\mathbf{c}_i)$
 - 6 $T \leftarrow T \cup \{\mathbf{c}_i \mapsto \mathbf{y}_i\}$ where T is cache table
 - 7 $\mathbf{c}_* \leftarrow \text{Search the nearest neighbor codevector to } \mathbf{x}_*^0 \text{ in } \text{OCH}_{\mathbf{X}}$
 - 8 $\mathbf{y}_* \leftarrow T(\mathbf{c}_*)$
 - 9 $\text{OCH}_{\mathbf{Y}} \leftarrow \text{Update } \text{OCH}_{\mathbf{Y}} \text{ for } \mathbf{y}_* \text{ with count } \alpha$
-

DBNN calculates the difference of prediction for a new data sample from the previous predictions. In the process, it executes DNN once if necessary, which is computationally expensive, in contrast to BNNs' repetitive execution DNNs. Furthermore, DBNN sometimes does not execute DNN, but only updates $\text{OCH}_{\mathbf{X}}$ and $\text{OCH}_{\mathbf{Y}}$ for the input and output vectors, by updating the counts and estimates prediction and uncertainty based on cached results. The dominant part of the computational cost of updating $\text{OCH}_{\mathbf{X}}$ is the inner product of a given input vector, i.e., $\mathbf{a} \cdot \mathbf{x}$, for nearest neighbor search. Given $\mathbf{x} = (\mathbf{x}^0, \mathbf{x}^1)$ and $\mathbf{a} = (\mathbf{a}^0, \mathbf{a}^1)$, $\mathbf{a} \cdot \mathbf{x} = \mathbf{a}^0 \cdot \mathbf{x}^0 + \mathbf{a}^1 \cdot \mathbf{x}^1$ holds. The codevector samples \mathbf{x}^1 from $\text{OCH}_{\mathbf{X}^1}$ is fixed and finite, and DBNN caches all $\mathbf{a}^1 \cdot \mathbf{x}^1$. Therefore, the average

Model	Throughput (fps)
U-Net	4.93
+ Softmax Probability	4.93
+ Model Uncertainty	0.154
+ Data Uncertainty	4.82
+ DBNN (<i>This work</i>)	4.80

Table 1: The number of video frames each model processes per second. The computational performance of DBNN is 3% lower than that of DNN and $31\times$ higher than that of BNN.

computational cost on $\mathbf{a}^1 \cdot \mathbf{x}^1$ is minuscule, when updating $\text{OCH}_{\mathbf{X}}$. In conclusion, the upper bound of the computational complexity of DBNN inference is $\mathcal{O}(\dim(\mathbf{x}^0) \log K_{\mathbf{X}} + \text{NN}(\cdot) + \dim(\mathbf{y}) \log K_{\mathbf{Y}})$ where $K_{\mathbf{X}}$ and $K_{\mathbf{Y}}$ are hyperparameters K of $\text{OCH}_{\mathbf{X}}$ and $\text{OCH}_{\mathbf{Y}}$, respectively. Modern NN performs vector operations dozens of times, if not hundreds, so the computation time of OCH is very small compared to DNN execution.

DBNN uses the flexible parametric probability estimator OCH to represent the distributions of input and output vector streams. Unlike the most BNNs that depend on a parameterized model described in (2), DBNN does not depend on the specific model. It is easy to convert DNN to BNN without significant modifications: just add OCH to the input and output of a DNN to estimate the probability of the input and output vector streams.

5 Experiments

We evaluate DBNN with semantic segmentation which is pixel-wise label classification. We use CamVid dataset [31] consisting of real-world day and dusk road scenes with 30 frame-per-second (fps) video sequence. The challenge is to segment each frame into 11 classes. Experimental results show that DBNN is 3% slower to process one video frame than DNN. The predictive performance of DBNN is 7% higher than that of DNN and 27% higher for ninety-percent certain pixels. The predictive performance of BNN is 11% higher than that of DNN and 33% higher for ninety-percent certain pixels, but BNN is 3100% slower than DNN.

We use the U-Net [32] as the backbone architecture with the VGG-16 [33] for the encoder and decoder. We implements the NNs using DL4J [34]. For all experiments, we train with 480×360 resized images of batch size 3 until the loss is saturated. We trained NNs with Adam with a constant learning rate of 0.001. All source code of DBNN is available at GitHub [35].

We compare the performance of the following four models against the deterministic U-Net:

- **Softmax Probability (SP).** Let $\max_l \text{Softmax}(z_l)$ be *softmax probability* where z is DNN logits and z_l is l -th element of z . It is easy to implement, but it differs from the actual classification probability when the NN is deepened, broadened, and regularized well [13].
- **Model Uncertainty (MU).** A model that takes only model uncertainty in DBNN is BNN, i.e., (1) and (3). Although it is difficult to determine analytically the number of samples that (3) converges, we use 30 samples, which is shown to be near optimal in [4].
- **Data Uncertainty (DU).** DBNN is configured to consider only data uncertainty, i.e., (8) with single weight $p(\mathbf{x}^1) = \delta(\mathbf{x}^1 - \mathbf{x}_*^1)$, not only show the effect of data uncertainty, but also shows how much DNN can achieve predictive uncertainty.
- **DBNN.** DBNN takes both data uncertainty and model uncertainty. We set hyperparameters K , λ , and $\sigma^{-1}(\phi)$ to 5, 5.0, and 1.0, respectively, in all OCHs of DBNN.

5.1 Computational Performance

Table 1 shows the number of video frames processed by each model per second on a NVIDIA TITAN Xp GPU. This table shows that DNN takes 203ms on average to process one frame. In comparison, DBNN takes 207ms on average to process one frame. The time to process OCH is 4.68ms, which is only 2% of the total. Since DU uses 30 samples to estimates uncertainty, DU is more than $30\times$ slower than DNN.

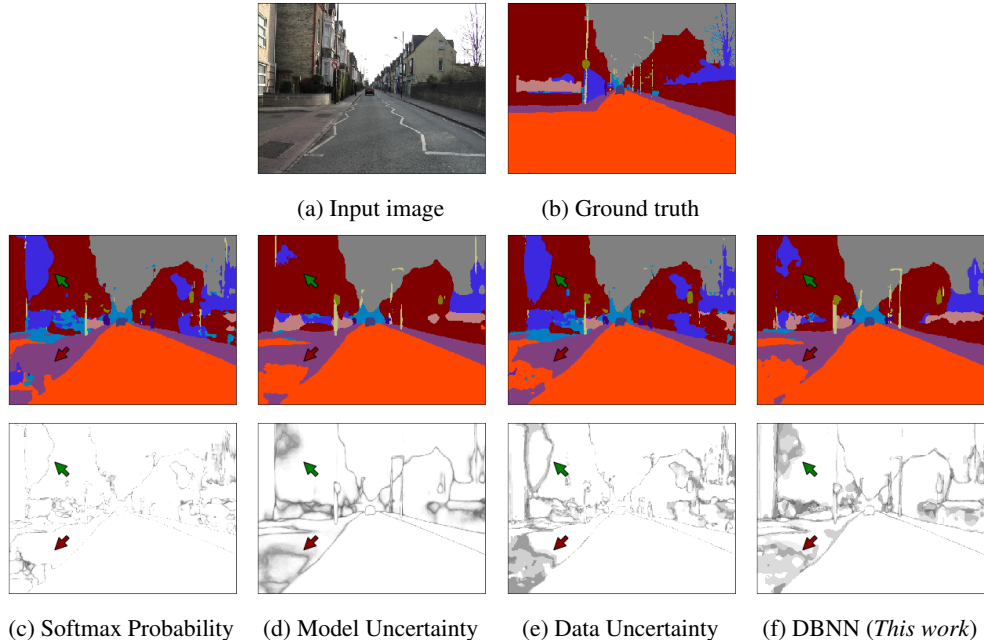


Figure 2: Quantitative results on the CamVid dataset for each model. In (c) to (f), the top is the predictive results and the bottom is the predictive uncertainty. A darker background corresponds to higher uncertainty. The areas indicated by the upper left and lower left arrows show different predictive uncertainty for misclassified region of each model.

Model	Accuracy	Accuracy-90	IoU	IoU-90	Coverage-90
U-Net	82.9	–	45.7	–	–
+ Softmax Probability	82.9	85.1	45.7	48.6	94.8
+ Model Uncertainty	84.2	91.0	49.8	60.0	83.9
+ Data Uncertainty	82.9	88.6	44.9	52.0	85.3
+ DBNN (<i>This work</i>)	83.7	91.0	47.7	56.7	81.1

Table 2: Predictive performance with semantic segmentation for each model. IoU for certain pixels of DBNN is 19% higher than IoU for all pixels. This result is compatible with the result that IoU for certain pixels of BNN is 20% higher than IoU for all pixels.

5.2 Predictive Performance

Figure 2 shows the qualitative comparison of the predictions for each model. SP is overconfident, i.e., uncertainty is generally low, and is mostly distributed at the boundaries of the classified chunks. Even when SP generates wrong prediction, arrowed in the result figure, the confidence level is very high. MU predicts a similar predictive result to ground truth than SP. The uncertainty is distributed on the boundaries as in the case of the softmax probability, but is also distributed in the misclassified areas. The predictive result of DU is similar to the result of SP. However, the uncertainty differs from the uncertainty of SP; First, DU is under-confident compared to softmax probability. Second, although DU does not identify all of the misclassifications compared to MU (upper left area), it sometimes estimates high uncertainty in the misclassified areas (lower left area). The predictive result and uncertainty of DBNN is similar to the model uncertainty as we expected.

Table 2 shows the quantitative comparison of the predictive performance for each model. We measure global pixel *accuracy* and mean intersection over unit (*IoU*). At the same time, we select only those pixels with confidence greater than 90% and measure the accuracy and IoU, called *accuracy-90* and *IoU-90*. We also measure the percentage of pixels with a confidence of 90% or more, called *coverage-90*.

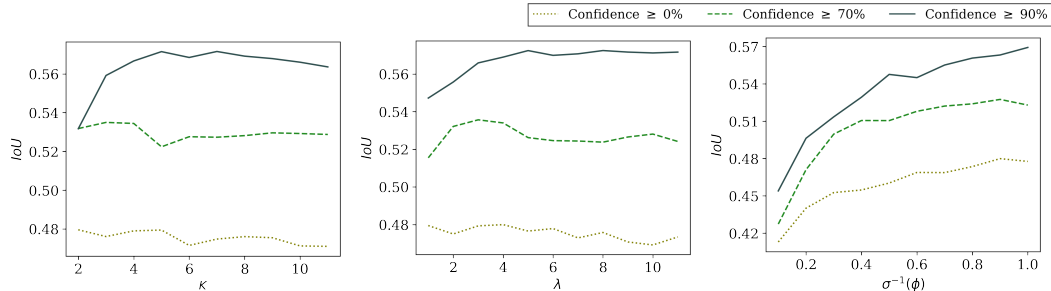


Figure 3: IoU for hyperparameters of OCH_Y , K , λ , and $\sigma^{-1}(\phi)$ (from left). The higher the value of K and λ , the higher the IoU until 5 and 5.0 respectively, and then the higher the value of K and λ , the lower the IoU.

MU, DU, and DBNN show 1.6%, -0.066%, and 0.97% higher accuracy than DNN, for all pixels, respectively. For pixels with ninety-percent or higher certainty, SP, MU, DU, and DBNN predicts with 2.6%, 8.1%, 6.9%, and 8.7% higher accuracy, respectively, compared to the accuracy for all pixels. MU and DBNN improves the accuracy more than SP and DU for confident pixels, which means that MU and DBNN estimates high uncertainty for misclassified region. IoUs for certain pixels increase by 6.3%, 20%, 16%, 19%, respectively, compared to the IoUs for all pixels, which shows the same trend as in accuracy. As shown in this results, SP is the most improper way to distinguish uncertain pixels because it has the least performance improvement compared to other methods for pixels with high confidence. On the other hand, MU has the highest performance improvement compared to DNN when considering all pixels, and it also has the highest performance improvement for certain pixels. DBNN has improved performance compared to DNN for all pixels, and has improved performance for certain pixels, similar to MU. The predictive performance of DU for all pixels is similar to the predictive performance of DNN, but for certain pixels, the performance is much better than that of SP.

5.3 Predictive Performance for Hyperparameters

DBNN takes three hyperparameters, i.e., K , λ , and $\sigma^{-1}(\phi)$, in the input and output OCHs. Figure 3 shows the IoUs for the hyperparameters of the output OCH. In this figure, the higher the value of K and λ , the higher the value of IoU until 5 and 5.0 respectively, and then the higher the value of K and λ , the lower the value of IoU. The higher the $\sigma^{-1}(\phi)$, the higher the IoU.

If K and λ are larger, DBNN maintains more codevectors — recent frames in video sequence. In this case, DBNN obtains more accurate model uncertainty using more codevectors. However, the data uncertainty is too high to estimate results. As a result, at low K and λ , IoU is low because model uncertainty is not precise. At high K and λ , IoU is low again because the data uncertainty increases and the assumption of DBNN is no longer held. IoU is maximized when model uncertainty and data uncertainty are balanced. On the other hand, if $\sigma^{-1}(\phi)$ is low, DBNN mostly adjusts the weights of codevectors and occasionally adds new codevectors. This results in the DBNN becoming inaccurate, but the calculation is faster. K and λ of input OCH did not affect the predictive performance. The effect of $\sigma^{-1}(\phi)$ of the input OCH is the same as that of the output OCH.

6 Conclusion

We present a differentiable BNN (DBNN) inference with respect to input data, which is a novel approximation of BNN inference, to improve the computational performance of BNN inference for data streams. In DBNN, we introduce a new term that is the probability of data streams in the BNN inference, and approximated it with a histogram for high-dimensional vector streams. Consequently, the DBNN inference executes DNN only once to calculate the prediction changed by a new data from data streams. This results in an order of magnitude times improvement in computational performance compared to BNN. Experiments with semantic segmentation using real-world datasets show that the computational performance of DBNN is almost the same as that of DNN, and uncertainty is comparable to that of BNN.

Acknowledgement

This work was supported by Samsung Research Funding Center of Samsung Electronics under Project Number SRFC-IT1801-10

References

- [1] Kaiming He, Xiangyu Zhang, Shaoqing Ren, and Jian Sun. Delving deep into rectifiers: Surpassing human-level performance on imagenet classification. In *The IEEE International Conference on Computer Vision (ICCV)*, December 2015.
- [2] David Silver, Aja Huang, Chris J Maddison, Arthur Guez, Laurent Sifre, George Van Den Driessche, Julian Schrittwieser, Ioannis Antonoglou, Veda Panneershelvam, Marc Lanctot, et al. Mastering the game of go with deep neural networks and tree search. *nature*, 529(7587):484, 2016.
- [3] Diego Ardila, Atilla P Kiraly, Sujeeth Bharadwaj, Bokyung Choi, Joshua J Reicher, Lily Peng, Daniel Tse, Mozziyar Etemadi, Wenxing Ye, Greg Corrado, David P Naidich, and Shravya Shetty. End-to-end lung cancer screening with three-dimensional deep learning on low-dose chest computed tomography. *Nature Medicine*, 2019.
- [4] Alex Kendall, Vijay Badrinarayanan, and Roberto Cipolla. Bayesian segnet: Model uncertainty in deep convolutional encoder-decoder architectures for scene understanding. *arXiv preprint arXiv:1511.02680*, 2015.
- [5] Alex Kendall and Yarin Gal. What uncertainties do we need in bayesian deep learning for computer vision? In *Advances in neural information processing systems*, pages 5574–5584, 2017.
- [6] Gregory Kahn, Adam Villaflor, Vitchyr Pong, Pieter Abbeel, and Sergey Levine. Uncertainty-aware reinforcement learning for collision avoidance. *arXiv preprint arXiv:1702.01182*, 2017.
- [7] Ian Osband, John Aslanides, and Albin Cassirer. Randomized prior functions for deep reinforcement learning. In *Advances in Neural Information Processing Systems*, pages 8617–8629, 2018.
- [8] Meire Fortunato, Charles Blundell, and Oriol Vinyals. Bayesian recurrent neural networks. *arXiv preprint arXiv:1704.02798*, 2017.
- [9] Jaesik Yoon, Taesup Kim, Ousmane Dia, Sungwoong Kim, Yoshua Bengio, and Sungjin Ahn. Bayesian model-agnostic meta-learning. In *Advances in Neural Information Processing Systems*, pages 7332–7342, 2018.
- [10] Chelsea Finn, Kelvin Xu, and Sergey Levine. Probabilistic model-agnostic meta-learning. In *Advances in Neural Information Processing Systems*, pages 9516–9527, 2018.
- [11] Alex Kendall, Yarin Gal, and Roberto Cipolla. Multi-task learning using uncertainty to weigh losses for scene geometry and semantics. In *Proceedings of the IEEE Conference on Computer Vision and Pattern Recognition*, pages 7482–7491, 2018.
- [12] Balaji Lakshminarayanan, Alexander Pritzel, and Charles Blundell. Simple and scalable predictive uncertainty estimation using deep ensembles. In *Advances in Neural Information Processing Systems*, pages 6402–6413, 2017.
- [13] Chuan Guo, Geoff Pleiss, Yu Sun, and Kilian Q Weinberger. On calibration of modern neural networks. In *Proceedings of the 34th International Conference on Machine Learning-Volume 70*, pages 1321–1330. JMLR. org, 2017.
- [14] José Miguel Hernández-Lobato and Ryan P Adams. Probabilistic Backpropagation for Scalable Learning of Bayesian Neural Networks. *NIPS*, stat.ML, 2015.
- [15] Yarin Gal and Zoubin Ghahramani. Dropout as a Bayesian Approximation - Representing Model Uncertainty in Deep Learning. *ICML*, 2016.
- [16] Matthew D Hoffman and Andrew Gelman. The no-u-turn sampler: adaptively setting path lengths in hamiltonian monte carlo. *Journal of Machine Learning Research*, 15(1):1593–1623, 2014.

- [17] Dustin Tran, Matthew W Hoffman, Dave Moore, Christopher Suter, Srinivas Vasudevan, and Alexey Radul. Simple, distributed, and accelerated probabilistic programming. In *Advances in Neural Information Processing Systems*, pages 7598–7609, 2018.
- [18] Patrick McClure and Nikolaus Kriegeskorte. Representing inferential uncertainty in deep neural networks through sampling. 2016.
- [19] Mattias Teye, Hossein Azizpour, and Kevin Smith. Bayesian uncertainty estimation for batch normalized deep networks. *arXiv preprint arXiv:1802.06455*, 2018.
- [20] Qiang Liu and Dilin Wang. Stein variational gradient descent: A general purpose bayesian inference algorithm. In *Advances In Neural Information Processing Systems*, pages 2378–2386, 2016.
- [21] Yuri Burda, Roger Grosse, and Ruslan Salakhutdinov. Importance weighted autoencoders. *arXiv preprint arXiv:1509.00519*, 2015.
- [22] Chris J Maddison, John Lawson, George Tucker, Nicolas Heess, Mohammad Norouzi, Andriy Mnih, Arnaud Doucet, and Yee Teh. Filtering variational objectives. In *Advances in Neural Information Processing Systems*, pages 6573–6583, 2017.
- [23] Christian A Naesseth, Scott W Linderman, Rajesh Ranganath, and David M Blei. Variational sequential monte carlo. *arXiv preprint arXiv:1705.11140*, 2017.
- [24] Tuan Anh Le, Maximilian Igl, Tom Rainforth, Tom Jin, and Frank Wood. Auto-encoding sequential monte carlo. *arXiv preprint arXiv:1705.10306*, 2017.
- [25] Aaron van den Oord, Oriol Vinyals, et al. Neural discrete representation learning. In *Advances in Neural Information Processing Systems*, pages 6306–6315, 2017.
- [26] Diederik P Kingma and Max Welling. Auto-encoding variational bayes. *arXiv preprint arXiv:1312.6114*, 2013.
- [27] Charles Blundell, Julien Cornebise, Koray Kavukcuoglu, and Daan Wierstra. Weight Uncertainty in Neural Networks. *arXiv.org*, May 2015.
- [28] R Gray. Vector quantization. *IEEE ASSP Magazine*, 1(2):4–29, 1984.
- [29] Allen Gersho. On the structure of vector quantizers. *IEEE Transactions on Information Theory*, 28(2):157–166, 1982.
- [30] Koji Kotani, Chen Qiu, and Tadahiro Ohmi. Face recognition using vector quantization histogram method. In *Proceedings. International Conference on Image Processing*, volume 2, pages II–II. IEEE, 2002.
- [31] Gabriel J Brostow, Julien Fauqueur, and Roberto Cipolla. Semantic object classes in video: A high-definition ground truth database. *Pattern Recognition Letters*, 30(2):88–97, 2009.
- [32] Olaf Ronneberger, Philipp Fischer, and Thomas Brox. U-net: Convolutional networks for biomedical image segmentation. In *International Conference on Medical image computing and computer-assisted intervention*, pages 234–241. Springer, 2015.
- [33] Karen Simonyan and Andrew Zisserman. Very deep convolutional networks for large-scale image recognition. *arXiv preprint arXiv:1409.1556*, 2014.
- [34] D Team et al. Deeplearning4j: Open-source distributed deep learning for the JVM. *Apache Software Foundation License*, 2, 2016.
- [35] Source codes of differential Bayesian Neural Network. <https://github.com/>, 2019.